

Theoretical investigation on the transition metal borides with Ta_3B_4 -type structure: a class of hard and refractory materials

Naihua Miao, Baisheng Sa, Jian Zhou, Zhimei Sun,*

Department of Materials Science and Engineering, College of Materials, Xiamen University, 361005 Xiamen, People's Republic of China

*Author to whom correspondence should be addressed. Tel and Fax: +86-592-2186664. Email addresses: zmsun@xmu.edu.cn and zhmsun2@yahoo.com.

Abstract

Based on density functional theory, we have systematically studied the structural stability, mechanical properties and chemical bonding of the transition metal borides M_3B_4 ($M=Ti, V, Cr, Zr, Nb, Mo, Hf, Ta, \text{ and } W$) for the first time. All the present studied M_3B_4 have been demonstrated to be thermodynamically and mechanically stable. The bulk modulus, shear modulus, Young's modulus, Poisson's ratio, microhardness, Debye temperature and anisotropy have been derived for ideal polycrystalline M_3B_4 aggregates. In addition, the relationship between Debye temperature and microhardness has been discussed for these isostructural M_3B_4 . Furthermore, the results of the Cauchy pressure, the ratio of bulk modulus to shear modulus, and Poisson's ratio suggest that the valence electrons of transition metals play an important role in the ductility of M_3B_4 . The calculated total density of states for M_3B_4 indicates that all these borides display a metallic conductivity. By analyzing the electron localization function, we show that the improvement of the ductility in these M_3B_4 might attribute to the decrease of their angular bonding character.

Keywords: Transition metal borides; Mechanical properties; Density functional theory; Electronic structure; Chemical bonding; Electron localization functions.

1. Introduction

Transition metal borides (TMBs) have been the focus of attention during the recent years due to their useful mechanical and electrical properties and their potential industrial applications (e.g. cutting tools and coatings). Among these TMBs, ReB_2 and OsB_2 are ultra-incompressible and superhard [1-3]; MgB_2 has been observed to be a superconductor at 39 K [4]; HfB_2 , ZrB_2 , MoB , CrB_2 , CrB , TiB_2 , Ti_3B_4 and TiB have been used as coatings or reinforcements in various composites because of their great hardness and good thermal stability [5-13]. As far as we know, most of the experimental works and theoretical studies are concentrated on the transition metal monoborides and diborides. While, another class of TMBs (M_3B_4) with Ta_3B_4 -type structure (Space Group IMMM, No.71) also exhibit great hardness [14-16], possess high melting point[16-18], show good electrical conductivity [14, 17, 18], and display considerable oxidation-resistant in air [16-18], which can be regarded as potentially useful materials for high temperature engineering applications, but insufficient attention was paid to them. Theoretical works on the electronic and bonding properties of Ta_3B_4 -type compounds have been carried out, but they were mainly performed for Ta_3B_4 [17]. A computational thermodynamic study on the stability of V_3B_4 suggested that it was stable enough as a refractory material for high temperature composite applications [19]. Experimentally, it has been shown that the platelet morphology of the Ti_3B_4 phase could improve the strength and toughness of the platelet composite [20], and the Ti_3B_4 and TiB_2 peritectic composite particulates have been in-situ synthesized to reinforce metal matrix composite [11]. Large crystals of Cr_3B_4 , Ta_3B_4 and related solid solutions have been prepared and measured to have a Vickers microhardness (H_v) around 22 GPa by Shigeru Okada *et al.* [14, 16]. A relatively larger H_v value of 33 ± 2 GPa has also been reported for Ta_3B_4 , indicating its

potential applications for nanostructured superhard materials [15]. However, up to now, due to the limited published works on M_3B_4 , the knowledge of these materials is rather scarce, e.g., their structural stability, mechanical properties and chemical bonding are still unknown. Therefore, a systematic investigation on this class of hard and refractory materials is of great practical interest and importance.

Computational technique based on density functional theory is a powerful tool to explore the phase stability and physical and mechanical properties of materials. In the present work, by means of density functional theory calculations, we focused on transition metal borides M_3B_4 ($M=Ti, V, Cr, Zr, Nb, Mo, Hf, Ta, \text{ and } W$). Among these borides, Hf_3B_4 and W_3B_4 have not yet been reported experimentally and their structural stabilities are still unknown. Hence, we began with our study on the thermodynamic stabilities of M_3B_4 (Section 3.1), and then systematically explored their mechanical properties (Section 3.2), Debye temperature (Section 3.3), anisotropy (Section 3.4), electronic structure and chemical bonding (Section 3.5), and dynamical stability (Section 3.6). Our results will provide a fundamental understanding on these hard and refractory materials and offer reference data for experimentalists. The remainder of the paper is organized as follows. In Section 2, we describe the computational methods and details. In Section 3, the results and discussions are presented. Finally, the conclusions are given in Section 4.

2. Calculation methods

The present calculations are based on the density functional theory (DFT). And there are 14 atoms for each cell, i.e., 8 boron atoms and 6 transition metal atoms.

Firstly, the Cambridge Serial Total Energy Package (CASTEP) [21] was used for geometry optimizations and elastic constants calculations. The interactions between

the ions and the electrons were described by using the Ultrasoft Vanderbilt pseudopotentials (USPP) [22]. The valence electrons were treated as: $2s2p$ for B; $3s3p3d4s$ for Ti, V and Cr; $4s4p4d5s$ for Zr, Nb and Mo; $5d6s$ for Hf, Ta; and $5s5p5d6s$ for W. The generalized gradient approximation (GGA) [23] and Perdew Burke Ernzerhof functional (PBE) [24] were employed for exchange correlation functional. The structures were optimized through the Broyden–Fletcher–Goldfarb–Shanno (BFGS) method [25]. A cutoff energy of 600 eV was chosen for plane wave basis set and the $12 \times 4 \times 12$ k-points were automatically generated by Monkhorst-Pack (MP) scheme [26]. The convergence criteria were set to maximum force tolerance within 0.03 eV/Å for geometry optimization, and 0.006 eV/Å for elastic constants calculations.

To obtain the force constants for phonon calculations and to check the reliability of results gained by CASTEP, the Vienna *ab initio* simulation package (VASP) code as implemented to solve the Kohn-Sham equations employing the projector augmented wave (PAW) method [27-30] was also used. The semi-core p states and possibly the semi-core s states were treated as valence states. PAW-GGA-PBE [23, 24, 29, 30] pseudopotentials with electronic configurations of B $2s^2 2p^1$, Ti $3p^6 3d^2 4s^2$, V $3p^6 3d^3 4s^2$, Cr $3p^6 3d^5 4s$, Zr $4s^2 4p^6 5s^2 4d^2$, Nb $4p^6 5s^2 4d^3$, Mo $4p^6 5s^1 4d^5$, Hf $5p^6 6s^2 5d^2$, Ta $5p^6 6s^2 5d^3$, and W $5p^6 6s^2 5d^4$ were employed. The cutoff energy for plane wave basis set was 700 eV. $12 \times 4 \times 12$ k-points and MP scheme [26] were adopted for Brillouin Zone sampling. The relaxation convergence for ions and electrons were 1×10^{-5} eV and 1×10^{-6} eV, respectively. The force constants, lattice parameters, density of states, and electron localization function (ELF) [31, 32] analyzed by VESTA [33] were calculated for the equilibrium structures.

Our phonon calculations were performed through the supercell approach [34]. Force constants of supercells were prepared by using the VASP, and the PHONOPY code [35, 36] was used to calculate the phonon frequencies and phonon density of states.

3. Results and discussions

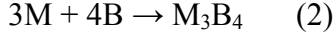
3.1. Lattice parameters and thermodynamic stability

The calculated lattice parameters of M_3B_4 are given in Table. 1. Note that the lattice constants predicted by CASTEP and VASP are in good agreement with each other and the available experimental data, indicating the reliability of the results obtained from the present density functional theory approaches. As seen from Table. 1, the predicted lattice constants of Ti_3B_4 , V_3B_4 and Nb_3B_4 are in good agreement with the experiments [37-39]. For Ta_3B_4 , the calculated lattice parameters are a bit larger than the experimental data (e.g., about 1.6% larger for b) [16], while for Cr_3B_4 , the calculated lattice constants are slightly smaller than the experiments (e.g., about 2.7% smaller for a) [40], which is within the GGA error. However, for the other compounds M_3B_4 such as Zr_3B_4 , Mo_3B_4 , Hf_3B_4 and W_3B_4 , there are no theoretical or experimental data available for comparison. Therefore, the present results could provide useful information for further experimental or theoretical investigations. From Table. 1, it is obvious that the lattice constants (a , b and c) follow the orders of $Ti_3B_4 < V_3B_4 < Cr_3B_4$ for $3d$ M_3B_4 , $Zr_3B_4 < Nb_3B_4 < Mo_3B_4$ for $4d$ M_3B_4 , and $Hf_3B_4 < Ta_3B_4 < W_3B_4$ for $5d$ M_3B_4 , which is reasonable as the radii of elements in the same row of the periodic table decrease with increasing atomic numbers. Moreover, we also observed that the predicted lattice parameters for Zr_3B_4 and Hf_3B_4 were a bit larger than the other M_3B_4 .

This can be understood as Zr and Hf possesses larger atomic radii than the other transition metals studied herein.

To investigate the possibility to obtain M_3B_4 , we have calculated the formation energy E_{form} by Eq. (1) according to the reaction (2).

$$E_{\text{form}} = E_{\text{total}}^{(M_3B_4)} - 3E_{\text{total}}^{(M)} - 4E_{\text{total}}^{(B)} \quad (1)$$



The total energy E_{total} of M and B were calculated for stable crystalline transition metals and α -boron, respectively. The results are also given in Table. 1. For all the M_3B_4 borides, the formation energies are negative, suggesting that all of them are thermodynamically stable. Hence, we expect that all of them, including two new compounds Hf_3B_4 and W_3B_4 , could be realized experimentally.

3.2. Mechanical properties

The mechanical properties of solids are of great importance because they relate to many properties of materials, e.g. interatomic potentials, equation of states, melting points and phonon spectra. Here, we start with the calculations of elastic constants.

3.2.1. Elastic constants

For orthorhombic M_3B_4 crystals, there are nine independent elastic constants which are usually referred to as c_{11} , c_{22} , c_{33} , c_{44} , c_{55} , c_{66} , c_{12} , c_{13} and c_{23} . In the present work, we obtained the elastic constants by applying a given homogeneous deformation (strain) and calculating the resulting stress [41] as implemented in CASTEP. The calculated elastic constants are presented in Table. 2. Among these borides, V_3B_4 exhibits the largest elastic constants of c_{22} , c_{33} , c_{44} , c_{55} , and c_{66} , while W_3B_4 possesses the largest elastic constants of c_{11} , c_{12} , c_{13} and c_{23} . As seen from Table. 2, c_{11} , c_{12} , c_{13} and c_{23} elastic constants increase with increasing valence electrons concentration (VEC), which indicates the valence electrons of transition metals in

M_3B_4 may play an important role in these elastic constants. For orthorhombic crystals, the Born mechanical stability criteria are given by: $c_{11}>0$, $c_{22}>0$, $c_{33}>0$, $c_{44}>0$, $c_{55}>0$, $c_{66}>0$, $(c_{11}+c_{22}-2c_{12})>0$, $(c_{11}+c_{33}-2c_{13})>0$, $(c_{22}+c_{33}-2c_{23})>0$, $(c_{11}+c_{22}+c_{33}+2c_{12}+2c_{13}+2c_{23})>0$. It is obvious that all of the studied M_3B_4 crystals with Ta_3B_4 -type structure satisfy the Born criteria, hence they are all mechanically stable.

3.2.2. Mechanical parameters for polycrystalline aggregates

From the calculated elastic constants, other mechanical parameters for polycrystalline aggregate such as bulk modulus (K), shear modulus (G), Young's modulus (E), and Poisson's ratio (σ) can be derived using Voigt–Reuss–Hill (VRH) approximation [42-44]. Voigt's and Reuss's schemes represent the upper and lower bounds to the elastic modulus, respectively. For orthorhombic crystals, the shear modulus (G) and the bulk modulus (K) according to Voigt and Reuss approximations are defined as:

$$G_V = \frac{1}{15}(c_{11} + c_{22} + c_{33} - c_{12} - c_{13} - c_{23}) + \frac{1}{5}(c_{44} + c_{55} + c_{66}) \quad (3)$$

$$K_V = \frac{1}{9}(c_{11} + c_{22} + c_{33}) + \frac{2}{9}(c_{12} + c_{13} + c_{23}) \quad (4)$$

$$G_R = \frac{15}{4(s_{11} + s_{22} + s_{33}) - 4(s_{12} + s_{13} + s_{23}) + 3(s_{44} + s_{55} + s_{66})} \quad (5)$$

$$K_R = \frac{1}{(s_{11} + s_{22} + s_{33}) + 2(s_{12} + s_{13} + s_{23})} \quad (6)$$

The Hill's averages are taken from the averages of the two [44]:

$$G = (G_V + G_R)/2 \quad (7)$$

$$K = (K_V + K_R)/2 \quad (8)$$

Then the Young's modulus (E), and Poisson's ratio (σ) are calculated by the following formulas:

$$E = 9KG/(3K + G) \quad (9)$$

$$\sigma = (3K - 2G)/2(3K + G) \quad (10)$$

Based on equations (3)-(10), we derived the corresponding values which are presented in Table. 3. As far as we know, there are no experimental results available related to the elastic modulus for M_3B_4 studied here, but we can compare these modulus with other known ceramic crystals. As seen from Table. 3, the bulk modulus K follow the orders of $Ti_3B_4 < V_3B_4 < Cr_3B_4$ for $3d$ M_3B_4 , $Zr_3B_4 < Nb_3B_4 < Mo_3B_4$ for $4d$ M_3B_4 , and $Hf_3B_4 < Ta_3B_4 < W_3B_4$ for $5d$ M_3B_4 , indicating that the increased extra valence electrons of transition metals contribute to the chemical bonding of M_3B_4 . And for all studied borides, their shear modulus ranging from 165 GPa to 238 GPa may reveal that there are strong directional bonding in these borides. Among them, V_3B_4 shows the largest shear modulus (238 GPa) and Young's modulus (555 GPa). The shear modulus of V_3B_4 is much larger than that of $\alpha-Al_2O_3$ (143 GPa) [45] and is comparable to that of stishovite (218 GPa) [45] and $\gamma-Si_3N_4$ (248 GPa) [45]. A largest bulk modulus value of 335 GPa for W_3B_4 is also observed in Table. 3, suggesting that W_3B_4 is very incompressible, which is about 11% lower compared with c-BN (376 GPa) [45] but much higher than $Ti_{0.25}Al_{0.75}N$ (178 GPa, the benchmark cutting tool material today) [46]. It is also noted in Table. 3 that, for all the borides studied here, their Poisson's ratio (σ) are very small, indicating all of them are relatively stable against shear. As is known, the range of Poisson's ratio for central-force solids are 0.25–0.5 [47, 48], thus, the interatomic forces are central in Mo_3B_4 and W_3B_4 , while they are non-central in the other M_3B_4 as their Poisson's ratio are all smaller than 0.25.

3.2.3. Microhardness

To estimate the microhardness (H_V) of M_3B_4 , we used the following relation for isotropic solids:

$$H_V = (1-2\sigma)E/[6(1+\sigma)] \quad (11)$$

The estimated microhardness H_V is also listed in Table. 3. Our estimated H_V values are ranging from 18.3 (W_3B_4) to 26.4 (V_3B_4) GPa indicating that all these M_3B_4 are hard materials. The calculated microhardness 23.9 GPa for Cr_3B_4 is in good agreement with the experimental value 21.9 ± 1.0 GPa [18]. For Ta_3B_4 , Shigeru Okada *et al* suggested that it had a same level of microhardness as Cr_3B_4 [16], which is consistent with our prediction. Nevertheless, when compared with the reported H_V 33 ± 2 GPa for Ta_3B_4 [15], our calculated H_V is a bit smaller. However, it should be noted that our estimated H_V 22.5 GPa for Ta_3B_4 is in the range of the values from 21.9 to 33 ± 2 GPa. From Table. 3, we can also observe that V_3B_4 shows the greatest microhardness value among these M_3B_4 borides. According to Teter [49], the polycrystalline shear modulus is a better predictor of hardness than bulk modulus, the microhardness can be calculated by: $H_T = 0.1769G - 2.899$. The result is also given in Table. 3, which is a bit larger than the data obtained from equation (11). Note that the later estimated microhardness H_T for Ta_3B_4 is in good agreement with the reported value 33 ± 2 GPa [15]. For both estimated microhardness H_V and H_T of M_3B_4 , the trends are quite similar, i.e., the higher shear modulus, the higher microhardness.

3.2.4. Ductility and brittleness

To explore the ductility and brittleness of M_3B_4 , we refer to the Cauchy pressure and the ratio of bulk modulus to shear modulus (K/G). Pettifor [50] has suggested that the angular character of atomic bonding in metals and compounds, which also relates to their brittleness or ductility, could be described by the Cauchy pressure. For directional bonding with angular character, the Cauchy pressure is negative, with

larger negative pressure representing a more directional character, which will be further explored in Section 3.5. Generally speaking, a positive Cauchy pressure reveals damage tolerance and ductility of a crystal, while a negative one demonstrates brittleness. In Fig. 1, the Cauchy pressures ($c_{23} - c_{44}$) for orthorhombic crystals as a function of valence electrons concentration (VEC) are illustrated for M_3B_4 . Clearly, for all M_3B_4 , where transition metal elements M are in the same rows ($3d$, $4d$, and $5d$), the Cauchy pressures increase with increasing VEC, i.e., $c_{23} - c_{44}$ follow the orders of $Ti_3B_4 < V_3B_4 < Cr_3B_4$ for $3d$ M_3B_4 , $Zr_3B_4 < Nb_3B_4 < Mo_3B_4$ for $4d$ M_3B_4 , and $Hf_3B_4 < Ta_3B_4 < W_3B_4$ for $5d$ M_3B_4 , indicating that the increased valence electrons of transition metals contribute to the ductility of M_3B_4 . As seen from Fig. 1, it is obvious that the Cauchy pressure for W_3B_4 is positive, suggesting the ductility of W_3B_4 , while for the other studied borides, their Cauchy pressures are all negative, showing that all of them have a brittle nature.

To qualify whether a material would fail in a ductile or brittle manner, Pugh proposed the ratio of bulk modulus to shear modulus (K/G) [51]. The transition from ductile to brittle behavior occurs around a K/G value of 1.75. Based on this assumption, materials with K/G values larger than 1.75 are associated with ductility, whereas materials with values smaller than 1.75 correspond to a brittle nature. The plot of K/G ratios as a function of valence electrons concentration (VEC) for M_3B_4 is given in Fig. 2. Compared with Fig. 1, a similar trend can be observed for K/G ratios and VEC, i.e., K/G ratios increase with VEC and also follow the orders of $Ti_3B_4 < V_3B_4 < Cr_3B_4$ for $3d$ M_3B_4 , $Zr_3B_4 < Nb_3B_4 < Mo_3B_4$ for $4d$ M_3B_4 , and $Hf_3B_4 < Ta_3B_4 < W_3B_4$ for $5d$ M_3B_4 . The calculated K/G value for W_3B_4 is 1.97, obviously larger than 1.75, indicating the ductile nature of W_3B_4 . This is in good agreement with the above discussion on the ductility of W_3B_4 . For the other M_3B_4 ,

their K/G values are all more or less smaller than 1.75, hence they can be classified as brittle materials.

As is known, Poisson's ratio has great correlation with ductility of crystalline alloys and amorphous metals, and it has been used as a screening parameter to identify intrinsic ductility of metals and alloys [52], i.e., the higher Poisson's ratio, the better ductility at low temperature, and vice versa. The Poisson's ratio as a function of valence electrons concentration (VEC) for M_3B_4 has also been given in Fig. 3. The trend for the relationship between Poisson's ratio and VEC is quite similar to that in Fig. 1 and Fig. 2, i.e., Poisson's ratio of M_3B_4 goes up with the increase of their VEC. As seen from Fig. 3, Ti_3B_4 possesses the smallest Poisson's ratio, and hence it shows the greatest brittleness among these M_3B_4 compounds. While W_3B_4 exhibits the largest Poisson's ratio indicating its greatest ductility. Furthermore, the brittleness of M_3B_4 follow the orders of $Ti_3B_4 > V_3B_4 > Cr_3B_4$ for $3d$ M_3B_4 , $Zr_3B_4 > Nb_3B_4 > Mo_3B_4$ for $4d$ M_3B_4 , and $Hf_3B_4 > Ta_3B_4 > W_3B_4$ for $5d$ M_3B_4 . These results coincide well with the above analysis of Cauchy pressures and K/G values.

3.3. Debye temperature

3.3.1. The calculation of Debye temperature

Mechanical properties can be related to thermodynamical parameters such as Debye temperature, specific heat, thermal expansion and melting point [48]. We have calculated the Debye temperature (θ_D) for M_3B_4 by the relation between the mean sound velocity v_m and θ_D [53]:

$$\theta_D = \frac{h}{k} \left[\frac{3n}{4\pi} \left(\frac{N_A \rho}{M} \right) \right]^{1/3} v_m \quad (12)$$

where h is Planck's constant, k is Boltzmann's constant, N_A is Avogadro's number, ρ is the density, M is the molecular weight and n is the number of atoms in the molecule.

The mean sound velocity of polycrystalline materials can be obtained according to the following approximations [53]:

$$v_m = \left[\frac{1}{3} \left(\frac{2}{v_t^3} + \frac{1}{v_l^3} \right) \right]^{-1/3} \quad (13)$$

where v_l and v_t are the longitudinal and transverse elastic wave velocity of the polycrystalline material which can be obtained by using the polycrystalline shear modulus G and the bulk modulus K from Navier's equation [54]:

$$v_l = \left(\frac{K + \frac{4G}{3}}{\rho} \right)^{1/2} \quad (14)$$

$$v_t = \left(\frac{G}{\rho} \right)^{1/2} \quad (15)$$

The calculated results are listed in Table. 4. Among these materials, V_3B_4 displays the highest Debye temperature of 1058 K, and about half of this value is obtained for W_3B_4 . For Nb_3B_4 , a theoretical θ_D of 592 K has been reported by Blinder and Bolgar [55], which is 209 K smaller than our predicted value 801K. Nevertheless, it should be noted that, by using the same approach [55], they also obtained other θ_D values of 339 K for HfB_2 (580 K [56]), 440 K for NbB_2 (720 K [56]) and 332 K for TaB_2 (570 K [56]), which are much smaller than the experimental data (where the experimental values are in the parenthesis). As their theoretical approach generally underestimated the Debye temperature, it is understandable that our calculated θ_D are higher than their predicted values. Therefore, although there is no other theoretical or experimental data available for comparison, we believe that our predicted θ_D for M_3B_4 are reasonable and can be used as reference for the experimentalists or theorists. For materials, usually, the higher Debye temperature, the larger microhardness.

Interestingly, in the present work, Hf_3B_4 , Ta_3B_4 and W_3B_4 show lower Debye temperature compared with Zr_3B_4 , but all of them are harder than Zr_3B_4 , which is quite different from the normal cases. Thus, it is worthy to discuss the relationship between θ_D and H_V which will be given in the following subsection.

3.3.2. The relationship between Debye temperature and microhardness

The strength of interatomic cohesive forces in solids is exhibited by such properties as compressibility, microhardness, and melting point [48, 57]. The stronger these forces are, the higher the Debye temperature is; and vice versa [58]. For isostructural groups of crystals, the relationship between Debye temperature (θ_D) and microhardness (H_V) can be defined as [59]:

$$\theta_D = p \times H_V^{1/2} V^{1/6} M^{-1/2} + q \quad (16)$$

where M is molar mass, V is molecular volume, and p and q are linear fitted parameters for specified crystal system. This relationship for M_3B_4 borides is illustrated in Fig. 4, where the data are taken from the preceding subsections. As seen from Fig. 4, the above relationship has been perfectly represented by using our predicted Debye temperature θ_D and microhardness H_V . The fitted parameters are 1826.13 for p , and 7.40 for q . And then these parameters were used to recalculate the H_V values for M_3B_4 by using the equation (16). Little deviation has been observed in Fig. 4 when these newly obtained microhardness values were compared with the H_V values in Table. 3. So according to the above relation (16), one can roughly estimate H_V' (θ_D') for a class of isostructural crystals by some given data, i.e., we can firstly obtain the parameters (p , q) by fitting several pairs of θ_D and H_V , and then calculate corresponding H_V' (θ_D') with a known θ_D' (H_V') value.

3.4. Anisotropy

The anisotropy of crystals affects the physical properties in different directions of solids, e.g. microcracks are induced in ceramics due to their anisotropy of the coefficient of thermal expansion and elastic anisotropy. Therefore, it is necessary to investigate the elastic anisotropy of M_3B_4 borides. The shear anisotropic factors, which provide a measure of the degree of anisotropy in the bonding between atoms in different planes, are given by:

$$A_1 = \frac{4c_{44}}{c_{11} + c_{33} - 2c_{13}} \quad \text{for the } \{100\} \text{ plane} \quad (17)$$

$$A_2 = \frac{4c_{55}}{c_{22} + c_{33} - 2c_{23}} \quad \text{for the } \{010\} \text{ plane} \quad (18)$$

$$A_3 = \frac{4c_{66}}{c_{11} + c_{22} - 2c_{12}} \quad \text{for the } \{001\} \text{ plane} \quad (19)$$

The calculated values of A_1 , A_2 and A_3 for M_3B_4 are listed in Table. 5. For an isotropic crystal, the values of A_1 , A_2 and A_3 equal to 1, while any value smaller or greater than 1 is a measure of the degree of shear anisotropy possessed by the crystal. As seen from Table. 5, none of the shear anisotropic factors comes up to 1, indicating the low anisotropy of M_3B_4 borides. Among them, W_3B_4 exhibits the largest anisotropic for all three planes, i.e., W_3B_4 possesses the highest degree of shear anisotropy for its $\{100\}$, $\{010\}$ and $\{001\}$ planes. Similar to W_3B_4 , Mo_3B_4 also exhibits large anisotropic factors for all three planes. On the contrary, Ti_3B_4 , V_3B_4 and Cr_3B_4 display low anisotropy for all their three planes. Zr_3B_4 , Nb_3B_4 , Mo_3B_4 , Hf_3B_4 , Ta_3B_4 and W_3B_4 show larger anisotropy in the $\{001\}$ plane than their $\{100\}$ and $\{010\}$ planes.

In additions, we have also adopted another way to measure the elastic anisotropy by using the percentage of anisotropy in the compression and shear introduced by Chung and Buessum [60], which are defined as:

$$A_K = \frac{K_V - K_R}{K_V + K_R} \quad (20)$$

$$A_G = \frac{G_V - G_R}{G_V + G_R} \quad (21)$$

For crystals, a value of zero denotes elastic isotropy and a value of 100% represents largest anisotropy. The percentage of bulk and shear anisotropies are also given in Table. 5. We observed that all the M_3B_4 possessed low bulk anisotropy as the values ranging from 0 to 0.5%. It is obvious that W_3B_4 and Mo_3B_4 exhibit relatively high shear anisotropies among these borides, while the values of their bulk anisotropies are small.

3.5. Electronic structure and chemical bonding

In order to gain better understanding of the electronic structure and chemical bonding of M_3B_4 , we have calculated the total density of states (TDOS), which are presented in Fig. 5. The calculated TDOS of Ta_3B_4 agrees well with the previous work [17]. Note that the TDOS of M_3B_4 in the same column show similar characters, and there are finite values at the Fermi Levels, indicating the metallic conductivity of M_3B_4 as observed by experiments [14, 18]. For all studied borides, their Fermi Levels locate at the shoulders of the peaks of TDOS, suggesting that all of them are stable [61], which is consistent with the previous discussion on their stability. Moreover, the Fermi Levels of M_3B_4 move from a lower energy level to a higher one, following the orders of $Ti_3B_4 < V_3B_4 < Cr_3B_4$, $Zr_3B_4 < Nb_3B_4 < Mo_3B_4$, and $Hf_3B_4 < Ta_3B_4 < W_3B_4$, which indicates that the increased valence electrons of transitions metals contribute to the bonding states in M_3B_4 and hence enhance their bulk modulus.

To further explore the chemical bonding of M_3B_4 , the topological analysis of the electron localization function (ELF) [31, 32] has been carried out, since it gives a rather quantitative picture on the chemical bonding of compounds and provides a

convenient mathematical framework enabling an unambiguous characterization of bonds. Contour plots of ELF on the (100) plane of M_3B_4 are illustrated in Fig. 6. Clearly, the B_1-Hf_1 , B_1-B_2 and B_2-B_3 covalent bonding of Hf_3B_4 with angular character can be observed in Fig. 6 (a), where the maximum ELF values between the bonded atoms are greater than 0.75. Moreover, as seen in Fig. 6 (a), two labeled regions P_1 and P_2 with relatively high ELF values are visible, and the ELF values of Hf_2-Hf_3 and Hf_2-Hf_1 bonding are obviously smaller than that of Hf_1-Hf_3 bond, which also indicates angular bonding character around Hf atoms in Hf_3B_4 . A quite different chemical bonding character for Ta_3B_4 and W_3B_4 can be seen in Fig. 6 (b) and (c). The angular B_1-Ta_1 , B_1-B_2 and B_2-B_3 covalent bonding in Ta_3B_4 are weakened compared with that in Hf_3B_4 , and they are further weakened in W_3B_4 , as characterized by the maximum ELF values or regions between the bonded atoms decreasing from Hf_3B_4 to Ta_3B_4 and to W_3B_4 . Furthermore, when comparing Fig. 6 (b) with Fig. 6 (a), it is observed that the P_1 region of Ta_3B_4 almost disappears and its P_2 region becomes weaker. While in Fig. 6 (c), both regions P_1 and P_2 vanish and the bonding among the nearest W atoms become homogeneous, suggesting a non-angular character of W-W bonding in W_3B_4 . Therefore, the angular character of B-B, M-B, M-M bonding is weakened from Hf_3B_4 to Ta_3B_4 and to W_3B_4 with the increasing of the extra valence electrons. The similar trend can be observed from the ELF plots for the other M_3B_4 , where the angular bonding character of M_3B_4 follow the orders of $Ti_3B_4 > V_3B_4 > Cr_3B_4$, $Zr_3B_4 > Nb_3B_4 > Mo_3B_4$, and $Hf_3B_4 > Ta_3B_4 > W_3B_4$. Hence, the decrease of angular bonding character in M_3B_4 might be the reason for the increase of Cauchy pressure and the improvement of their ductility as seen in Section 3.2.

3.6. Dynamical stability

In the preceding subsections, we have demonstrated that all of the studied M_3B_4 are thermodynamically and mechanically stable. To further investigate the dynamical stability of two new predicted compounds Hf_3B_4 and W_3B_4 , we calculated phonon dispersions for them, which are illustrated in Fig.7 (a) and (b). The phonon dispersion curves of Hf_3B_4 and W_3B_4 are a little complex and show different characters. It is known that negative or imaginary frequencies indicate the dynamical instability of crystals. As seen from the phonon dispersion curves, no negative frequency have been found for Hf_3B_4 or W_3B_4 , suggesting both compounds are dynamically stable.

4. Concluding remarks

In summary, by means of density functional theory calculations, we have systematically study the structural stability, mechanical properties, electronic structure and chemical bonding of M_3B_4 (M are IVB, VB and VIB transition metals, i.e., M=Ti, V, Cr, Zr, Nb, Mo, Hf, Ta, and W). All the studied transition-metal borides with Ta_3B_4 -type structure are thermodynamically and mechanically stable. The predicted lattice parameters and microhardness for them are in good agreement with the available experimental results.

The bulk modulus, Young's modulus, shear modulus, Poisson's ratio, microhardness and Debye temperature have been derived from the calculated elastic constants for ideal polycrystalline M_3B_4 aggregates. Among them, V_3B_4 exhibits the highest shear modulus (238 GPa), Young's modulus (555 GPa), microhardness (26.4 GPa) and Debye temperature (1059 K), while W_3B_4 possesses the largest bulk modulus (335 GPa) but the lowest Debye temperature (532 K). In addition, the relationship between Debye temperature and microhardness has been discussed for these isostructural M_3B_4 . Furthermore, by analyzing the Cauchy pressure, the ratio of

bulk modulus to shear modulus, and Poisson's ratio, we found that the ductility of M_3B_4 follows the orders of $Ti_3B_4 < V_3B_4 < Cr_3B_4$, $Zr_3B_4 < Nb_3B_4 < Mo_3B_4$, and $Hf_3B_4 < Ta_3B_4 < W_3B_4$, suggesting that the valence electrons of transition metals play an important role in the ductility of M_3B_4 , i.e., the more valence electrons, the better ductility.

Moreover, the calculated total density of states of M_3B_4 indicates that all these borides display a metallic conductivity, and the increased valence electrons of transition metals contribute to the bonding states in M_3B_4 and hence enhance their bulk modulus. By analyzing the electron localization function, in the view of chemical bonding, we show that the decrease of angular bonding character in M_3B_4 might be the reason for the increase of Cauchy pressure and the improvement of their ductility. Finally, the calculated phonon dispersions of the new predicted compounds Hf_3B_4 and W_3B_4 suggest that both of them are dynamically stable. We expect our results provide a fundamental understanding on these hard and refractory materials and offer reference data for further investigation or applications of this class of transition metals borides.

Acknowledgements

This work is supported by National Natural Science Foundation of China (60976005), the Outstanding Young Scientists Foundation of Fujian Province of China (2010J06018) and the program for New Century Excellent Talents in University (NCET-08-0474). The State Key Laboratory for Physical Chemistry of Solid Surfaces at Xiamen University is greatly acknowledged for providing the computing resources.

References

- [1] H. Chung, M. Weinberger, J. Levine, A. Kavner, J. Yang, S. Tolbert and R. Kaner, *Science* **316** (2007), p. 436.
- [2] J.B. Levine, J.B. Betts, J.D. Garrett, S.Q. Guo, J.T. Eng, A. Migliori and R.B. Kaner, *Acta Mater.* **58** (2010), p. 1530.
- [3] X.Q. Chen, C. Fu, M. Krmar and G.S. Painter, *Phys. Rev. Lett.* **100** (2008), p. 196403.
- [4] D. Larbalestier, L. Cooley, M. Rikel, A. Polyanskii, J. Jiang, S. Patnaik, X. Cai, D. Feldmann, A. Gurevich and A. Squitieri, *Nature* **410** (2001), p. 186.
- [5] D. Sciti, S. Guicciardi and M. Nygren, *J. Am. Ceram. Soc.* **91** (2008), p. 1433.
- [6] N.L. Okamoto, M. Kusakari, K. Tanaka, H. Inui and S. Otani, *Acta Mater.* **58** (2010), p. 76.
- [7] D. Kalish, E. Clougherty and K. Kreder, *J. Am. Ceram. Soc.* **52** (2006), p. 30.
- [8] M. Zhang, H. Wang, H. Wang, T. Cui and Y. Ma, *J. Phys. Chem. C* **114** (2010), p. 6722.
- [9] M. Audronis, P. Kelly, A. Leyland and A. Matthews, *Thin Solid Films* **515** (2006), p. 1511.
- [10] K. Panda and K. Chandran, *Acta Mater.* **54** (2006), p. 1641.
- [11] J. Xu, Y. Kan and W. Liu, *Surf. Rev. Lett.* **12** (2005), p. 561.
- [12] L. Scatteia, D. Alfano, F. Monteverde, J.-L. Sans and M. Balat-Pichelin, *J. Am. Ceram. Soc.* **91** (2008), p. 1461.
- [13] D. Tzeli and A. Mavridis, *J. Chem. Phys.* **128** (2008), p. 034309.
- [14] S. Okada, Y. Yu, K. Kudou, T. Shishido, T. Tanaka, I. Higashi, T. Lundström and T. Fukuda, *J. Solid State Chem.* **154** (2000), p. 45.
- [15] R. Andrieviski, *Int. J. Refract. Met. Hard Mater.* **19** (2001), p. 447.
- [16] S. Okada, K. Kudou, I. Higashi and T. Lundström, *J. Cryst. Growth* **128** (1993), p. 1120.
- [17] R. Minyaev and R. Hoffmann, *Chem. Mater.* **3** (1991), p. 547.
- [18] S. Okada, K. Kudou, K. Iizumi, K. Kudaka, I. Higashi and T. Lundström, *J. Cryst. Growth* **166** (1996), p. 429.
- [19] H. Wiedemeier and M. Singh, *J. Mater. Sci* **26** (1991), p. 2421.
- [20] D. Brodtkin, S. Kalidindi, M. Barsoum and A. Zavaliangos, *J. Am. Ceram. Soc.* **79** (1996), p. 1945.
- [21] M. Segall, P. Lindan, M. Probert, C. Pickard, P. Hasnip, S. Clark and M. Payne, *J. Phys.: Condens. Matter* **14** (2002), p. 2717.
- [22] D. Vanderbilt, *Phys. Rev. B* **41** (1990), p. 7892.
- [23] J.P. Perdew and Y. Wang, *Phys. Rev. B* **45** (1992), p. 13244.
- [24] J.P. Perdew, K. Burke and M. Ernzerhof, *Phys. Rev. Lett.* **77** (1996), p. 3865.
- [25] T. Fischer and J. Almlof, *J. Phys. Chem.* **96** (1992), p. 9768.
- [26] H.J. Monkhorst and J.D. Pack, *Phys. Rev. B* **13** (1976), p. 5188.
- [27] G. Kresse and J. Furthmüller, *Phys. Rev. B* **54** (1996), p. 11169.
- [28] G. Kresse and J. Furthmüller, *Comput. Mater. Sci.* **6** (1996), p. 15.
- [29] P.E. Blöchl, *Phys. Rev. B* **50** (1994), p. 17953.
- [30] G. Kresse and D. Joubert, *Phys. Rev. B* **59** (1999), p. 1758.
- [31] B. Silvi and A. Savin, *Nature* **371** (1994), p. 683.
- [32] A. Savin, R. Nesper, S. Wengert and T.F. Fassler, *Angew. Chem. Int. Ed. Engl.* **36** (1997), p. 1808.
- [33] K. Momma and F. Izumi, *J. Appl. Cryst.* **41** (2008), p. 653.
- [34] K. Parlinski, Z.Q. Li and Y. Kawazoe, *Phys. Rev. Lett.* **78** (1997), p. 4063.
- [35] A. Togo, *Phonopy*, <http://phonopy.sourceforge.net/>.
- [36] A. Togo, F. Oba and I. Tanaka, *Phys. Rev. B* **78** (2008), p. 134106.
- [37] K. Spear, P. McDowell and F. McMahon, *J. Am. Ceram. Soc.* **69** (1986).
- [38] K. Spear, P. Liao and J. Smith, *J. Phase Equil.* **8** (1987), p. 447.
- [39] A. Bolgar, M. Serbova, T. Serebryakova, L. Isaeva and V. Fesenko, *Powder Metall. Met. Ceram.* **22** (1983), p. 207.
- [40] P. Liao and K. Spear, *J. Phase Equil.* **7** (1986), p. 232.
- [41] Z. Sun, R. Ahuja and J.E. Lowther, *Solid State Commun.* **150** (2010), p. 697.
- [42] W. Voigt, *Lehrbuch der Kristallphysik*, B.G. Teubner, Leipzig. (1928).
- [43] A. Reuss, *Z. Angew. Math. Mech.* **9** (1929), p. 49.
- [44] R. Hill, *Proc. Phys. Soc. London* **65** (1952), p. 349.
- [45] H. Yao, L. Ouyang and W. Ching, *J. Am. Ceram. Soc.* **90** (2007), p. 3194.

- [46] J. Emmerlich, D. Music, M. Braun, P. Fayek, F. Munnik and J. Schneider, *J. Phys. D* **42** (2009), p. 185406.
- [47] M.H. Ledbetter, *Materials at Low Temperatures. American Society for Metals, Metals Park, OH;* (1983).
- [48] P. Ravindran, L. Fast, P. Korzhavyi, B. Johansson, J. Wills and O. Eriksson, *J. Appl. Phys.* **84** (1998), p. 4891.
- [49] D. Teter, *MRS Bull.* **23** (1998), p. 22.
- [50] D. Pettifor, *Mater. Sci. Technol.* **8** (1992), p. 345.
- [51] S.F. Pugh, *Philos. Mag.* **45** (1954), p. 823.
- [52] M. Gao, N. Do an, P. King, A. Rollett and M. Widom, *J. Miner. Met. Mater. Soc.* **60** (2008), p. 61.
- [53] O.L. Anderson, *J. Phys. Chem. Solids* **24** (1963), p. 909.
- [54] E. Schreiber, Anderson O.L. and Soga N., *Elastic Constants and their Measurements. New York: McGraw-Hill;* (1973).
- [55] A. Blinder and A. Bolgar, *Powder Metall. Met. Ceram.* **30** (1991), p. 1053.
- [56] D. Steinberg, *Le Journal de Physique IV* **1** (1991), p. 3.
- [57] J. Plendl, S. Mitra and P. Gielisse, *Phys. Status Solidi B* **12** (1965), p. 367.
- [58] S. Abrahams and F. Hsu, *J. Chem. Phys.* **63** (1975), p. 1162.
- [59] P. Deus and H. Schneider, *Cryst. Res. Technol.* **18** (1983), p. 491.
- [60] D.H. Chung and W.R. Buessem, *Anisotropy in Single Crystal Refractory Compound (edited by F. W. Vahldiek and S. A. Mersol)* **2** (1968), p. 217.
- [61] Z. Sun, R. Ahuja and J.M. Schneider, *Phys. Rev. B* **68** (2003), p. 224112.

FIGURE CAPTIONS:

Fig. 1. (Color online) Plot for Cauchy pressure as a function of valence electron concentration (VEC).

Fig. 2. (Color online) Plot for K/G as a function of valence electron concentration (VEC).

Fig. 3. (Color online) Plot for Poisson's ratio as a function of valence electron concentration (VEC).

Fig. 4. The relationship between Debye temperature and microhardness H_v . The data points in squares are calculated using the data from the preceding sections.

Fig. 5. The calculated total density of states for M_3B_4 . The Fermi Levels have been set to 0 eV and marked by short dash lines.

Fig. 6. (Color online) Contour plots of ELF on the (100) plane of M_3B_4 for (a) Hf_3B_4 , (b) Ta_3B_4 , (c) W_3B_4 . The color scale for the ELF value is given at the left of the figure, where all the mappings are under the same saturation levels and the interval between two nearest contour lines is 0.13.

Fig. 7. The calculated phonon dispersion curve for (a) Hf_3B_4 and (b) W_3B_4 .

Table. 1. The calculated lattice parameters (a , b and c) and formation energy (E_{form}) for M_3B_4 . US and PAW denote the results obtained from CASTEP and VASP; Exp. represents the experimental data.

M_3B_4		$a(\text{\AA})$	$b(\text{\AA})$	$c(\text{\AA})$	$E_{\text{form}} (\text{eV/cell})$
Ti_3B_4	US	3.260	13.733	3.036	-13.470
	PAW	3.263	13.755	3.042	-
	Exp.[37]	3.259	13.730	3.032	-
V_3B_4	US	3.041	13.200	2.976	-11.826
	PAW	3.043	13.221	2.981	-
	Exp.[38]	3.03	13.18	2.986	-
Cr_3B_4	US	2.918	13.004	2.936	-6.870
	PAW	2.923	13.030	2.942	-
	Exp.[40]	2.99	13.010	2.949	-
Zr_3B_4	US	3.539	14.903	3.206	-12.071
	PAW	3.553	14.943	3.217	-
	Exp.	-	-	-	-
Nb_3B_4	US	3.307	14.103	3.144	-11.494
	PAW	3.325	14.179	3.159	-
	Exp.[39]	3.296	14.094	3.151	-
Mo_3B_4	US	3.161	13.900	3.074	-6.561
	PAW	3.175	13.974	3.086	-
	Exp.	-	-	-	-
Hf_3B_4	US	3.522	14.731	3.205	-11.382
	PAW	3.502	14.679	3.188	-
	Exp.	-	-	-	-
Ta_3B_4	US	3.332	14.227	3.176	-10.183
	PAW	3.309	14.091	3.145	-
	Exp.[16]	3.291	13.994	3.133	-
W_3B_4	US	3.185	13.923	3.073	-4.054
	PAW	3.196	13.993	3.083	-
	Exp.	-	-	-	-

Table. 2. The calculated elastic stiffness constants c_{ij} (in GPa) for M_3B_4 .

M_3B_4	c_{11}	c_{22}	c_{33}	c_{44}	c_{55}	c_{66}	c_{12}	c_{13}	c_{23}
Ti ₃ B ₄	424	520	581	229	242	214	108	94	49
V ₃ B ₄	484	640	631	239	264	236	137	140	96
Cr ₃ B ₄	492	609	612	231	238	205	169	166	159
Zr ₃ B ₄	372	357	458	184	162	183	114	79	78
Nb ₃ B ₄	473	546	544	201	242	236	157	168	126
Mo ₃ B ₄	484	476	559	208	219	196	227	202	193
Hf ₃ B ₄	419	432	523	208	225	212	128	117	90
Ta ₃ B ₄	479	559	552	196	232	233	170	182	150
W ₃ B ₄	507	459	556	205	223	200	271	225	253

Table. 3. The calculated Young's modulus (K_V , K_R , and K in GPa), shear modulus (G_V , G_R , and G in GPa), elastic modulus (E in GPa), Poisson's ratio (σ) and microhardness (H_V and H_T in GPa) for polycrystalline M_3B_4 aggregates.

M_3B_4	K_V	K_R	K	G_V	G_R	G	E	σ	H_V	H_T
Ti ₃ B ₄	225	224	224	222	217	220	497	0.131	24.4	36.0
V ₃ B ₄	278	275	277	240	236	238	555	0.166	26.4	39.2
Cr ₃ B ₄	300	298	299	216	213	215	520	0.210	23.9	35.1
Zr ₃ B ₄	192	191	192	167	163	165	385	0.166	18.3	26.3
Nb ₃ B ₄	274	273	274	210	205	208	497	0.197	23.1	33.8
Mo ₃ B ₄	307	306	307	184	177	181	453	0.254	20.1	29.1
Hf ₃ B ₄	227	226	227	198	194	196	457	0.165	21.8	31.8
Ta ₃ B ₄	288	288	288	205	201	203	493	0.215	22.5	33.0
W ₃ B ₄	336	335	335	177	163	170	437	0.283	18.9	27.2

Table. 4. The calculated density (ρ in g/cm^3), the longitudinal, transverse and mean elastic wave velocity (v_l , v_t and v_m in m/s), and the Debye temperature (θ_D in K) for M_3B_4 .

M_3B_4	ρ	v_l	v_t	v_m	θ_D
Ti_3B_4	4.57	10642	6935	7603	1055
V_3B_4	5.45	10437	6607	7268	1059
Cr_3B_4	5.94	9928	6012	6645	991
Zr_3B_4	6.22	8133	5148	5663	735
Nb_3B_4	7.29	8687	5334	5887	801
Mo_3B_4	8.14	8203	4713	5234	732
Hf_3B_4	11.56	6499	4118	4530	591
Ta_3B_4	12.93	6572	3959	4378	590
W_3B_4	14.50	6227	3426	3819	532

Table. 5. The calculated shear anisotropic factors (A_1 , A_2 , and A_3) for different planes and the percentage of anisotropy in the compression and shear (A_K and A_G).

M_3B_4	A_1	A_2	A_3	$A_K(\%)$	$A_G(\%)$
Ti ₃ B ₄	1.122	0.964	1.175	0.306	0.989
V ₃ B ₄	1.143	0.978	1.110	0.415	0.856
Cr ₃ B ₄	1.195	1.053	1.073	0.415	0.598
Zr ₃ B ₄	1.095	0.982	1.462	0.191	1.107
Nb ₃ B ₄	1.182	1.153	1.336	0.055	1.070
Mo ₃ B ₄	1.300	1.347	1.554	0.095	1.948
Hf ₃ B ₄	1.175	1.164	1.425	0.222	1.169
Ta ₃ B ₄	1.177	1.145	1.334	0.107	0.990
W ₃ B ₄	1.335	1.753	1.876	0.083	4.045